Published online 9 April 2009

Nucleic Acids Research, 2009, Vol. 37, No. 11 ***3625–3634***
doi:10.1093/nar/gkp216

Dramatic effect of single-base mutation on the conformational dynamics of human telomeric G-quadruplex

Ja Yil Lee[1,*] and D. S. Kim[1,2]

[1]Department of Physics and Astronomy and [2]Centre for Subwavelength Optics, Seoul National University, San 56-1, Shillim-dong, Kwanak-gu, Seoul, 151-742, South Korea

Received December 12, 2008; Revised February 23, 2009; Accepted March 17, 2009

ABSTRACT

Guanine-rich DNA sequences can form G-quadruplexes. These four-stranded structures are known to form in several genomic regions and to influence certain biological activities. Sometimes, the instability of G-quadruplexes causes the abnormal biological processes. Mutation is a culprit for the destabilization of G-quadruplexes, but the details of mutated G-quadruplexes are poorly understood. In this article, we investigated the conformational dynamics of single-base mutated human telomeric G-quadruplexes in the presence of K^+ with single-molecule FRET spectroscopy. We observed that the replacement of single guanine by thymine in a G-track induces various folded structures, i.e. structural polymorphism. Moreover, direct observation of their dynamics revealed that a single-base mutation causes fast unfolding of folded states under physiological conditions. Furthermore, we found that the degree of destabilization varies according to mutation positions. When the central guanine of a G-track is replaced, the G-quadruplexes unfold quickly at any K^+ concentrations and temperature. Meanwhile, outer-quartet mutated G-quadruplexes have heterogeneous dynamics at intermediate K^+ concentrations and longstanding folded states at high K^+ concentrations. Several factors such as base-stacking interaction and K^+ coordination are responsible for the different dynamics according to the mutation position.

INTRODUCTION

G-rich single-stranded DNA can form, *in vitro*, novel four-stranded structures, called G-quadruplexes. Great attention has been paid to G-quadruplexes because of their peculiar structure and biological significance, and numerous physicochemical properties about them have been revealed (1–5). Moreover, it was reported that they are formed *in vivo* (6–8). The G-quadruplex structures are believed to be formed in telomeres because telomeric DNA terminates with a single strand composed of G-rich tandem repeats that are beyond the double-stranded region (9,10). Telomeres protect chromosomes from degradation by exonucleases and maintain their integrity (11). In addition, telomeres are known to be closely related to the cancer (12,13). The human telomeric G-quadruplexes are thought to be potential anti-cancer targets because their novel structures inhibit the activity of telomerases, which are known to proliferate in cancer cells (12–15). Besides telomeres, quadruplex-forming sequences have been identified in several genomic regions involved in DNA metabolism (16–19). The instability of the potential G-quadruplexes may hinder normal cellular activities and cause biological abnormalities. The disruption of G-quadruplexes in insulin mini-satellite induced by mutation lowers the transcriptional activity of the insulin gene (19). Mutation in c-MYC promoter would disturb the G-quadruplexes and hence lead to over-expression of the proto-oncogene (20).

Recently, the effect of a methylated guanine in a G-track on the stability of human telomeric G-quadruplexes was examined (21). Results showed that methylation not only lowers stability of G-quadruplexes but also changes their folded structures. While this work provides useful information on the stability of the single-base mutated G-quadruplexes, it does not clearly describe the details of their instability. Also, a human telomeric DNA motif (HTDM) with mutation was examined in our previous work by using single molecule FRET spectroscopy (22). But the details were not systematically examined. In this article, we investigate the conformational dynamics of single-base mutated human telomeric G-quadruplexes and compared the central-G mutated (c-mut) and side-G mutated (s-mut) HTDMs in the presence of K^+, because potassium ions are plentiful inside cells (23) and play a crucial role in quadruplex formation (3,4). We used

*To whom correspondence should be addressed. Tel: +82 2 889 1295; Fax: +82 2 884 3002; Email: jayil@phya.snu.ac.kr

single-molecule FRET spectroscopy because the technique enables to exclude the ensemble averaged effects and to observe the dynamics of individual biomolecules in real time (24–26). For the single-base mutation in the human telomeric G-quadruplex, one guanine in a G-track was replaced by thymine. The single-molecule FRET spectroscopy revealed that the mutated human telomeric DNA motifs (HTDMs) exhibit structural polymorphism. The mutation causes short unfoldings of folded states even at the physiological salt concentration. Furthermore, the dynamic behavior is sensitive to mutation position.

MATERIALS AND METHODS

DNA preparation

A schematic sample configuration is depicted in Figure 1A. This sample is identical to the previous ones except that its sequence contains a single-point mutation (22,27). Two kinds of oligomers were synthesized (IDT Technology): G-quadruplex strand and stem strand. In the stem strand, tetramethylrhodamine (TMR) was internally labeled via amino C6 dT (**T***) for donor; [stem]: 5′-CGC ACC GTG GCC ATT ATC CTT **T***TA CCT CT-3′. The G-quadruplex strand is composed of the complementary strand to the stem strand and the human telomeric DNA motif (HTDM). To obtain the single-base mutated samples, we replaced each guanine in the third G-track by thymine (bold) in the HTDMs (underlined). The following sequences define the G-quadruplex strand: [wild-type]: 5′-Cy5-GGG TTA GGG TTA GGG TTA GGG AGA GGT AAA AGG ATA ATG GCC ACG GTG CG-biotin-3′, [c-mut]: 5′-Cy5-GGG TTA GGG TTA G**T**G TTA GGG AGA GGT AAA AGG ATA ATG GCC ACG GTG CG-biotin-3′, [s-mut1]: 5′-Cy5-GGG TTA GGG TTA **T**GG TTA GGG AGA GGT AAA AGG ATA ATG GCC ACG GTG CG-biotin-3′, and [s-mut2]: 5′-Cy5-GGG TTA GGG TTA GG**T** TTA GGG AGA GGT AAA AGG ATA ATG GCC ACG GTG CG-biotin-3′. In this strand, Cy5 was labeled at 5′ end for acceptor and biotin was modified at 3′ end for the surface attachment. All oligomers were dissolved in T50 [10 mM Tris–HCl (pH 7.4) and 50 mM NaCl]. The G-quadruplex strand and the stem strand were mixed in a 2:1 ratio. The mixture was heated to 95°C and then cooled to room temperature slowly. For ensemble circular dichroism (CD) measurements, only G-quadruplex motifs without fluorophores and biotin (underlined part) were synthesized to remove any effects of labeling and stem strands on CD spectra.

Ensemble CD and FRET measurements

A Jasco J-715 spectropolarimeter was used for CD measurements at room temperature (23°C). Total 5 μM of samples were prepared in a buffer with 10 mM Tris–HCl (pH 7.4) and 200 mM K^+. The scan range was from 220 to 320 nm with 1 nm resolution. For ensemble FRET measurements at room temperature, fluorescence of the annealed samples (200 nM) was measured with a spectrofluorometer (F-4500, Hitachi) at various K^+ concentrations. The samples were excited at 532 nm and the emission was scanned from 550 to 750 nm. The data were normalized by a donor (TMR) fluorescence peak at 580 nm.

Single-molecule experiments

A prism-type total internal reflection system was used for the single-molecule FRET imaging (24). A microchamber was made by first bonding a cleaned quartz slide and a coverslip with double-sided tape and then was treated with biotinylated BSA (1 mg/ml, Sigma) and streptavidin (0.2 mg/ml, Molecular Probe) successively. Next, ~100 pM of annealed DNA samples were injected into the chamber. T50 was used to wash the chamber between each step. Imaging buffer [10 mM Tris–HCl (pH 7.4), 0.4% (w/w) glucose, 1% 2-mercaptoethanol, 0.1 mg/ml glucose oxidase (G-2133, Sigma) and 0.02 mg/ml catalase (106810, Roche)] was used to reduce the photobleaching of dyes enzymatically (24,28). The fluorescence of individual DNA samples was collected by an objective lens (60×, N.A. 1.2, Olympus), dissected by a dichroic mirror (630DCXR, Chroma Technology), and then imaged on an intensified CCD (iXon, Andor) with 0.1 s exposure time. Recorded images were processed by commercial software (IDL, RSI). All experiments were performed at room temperature (23°C) unless the temperature is specifically mentioned. For temperature-dependent experiments, the sample temperature was controlled by a home-made thermal controller with ±1°C resolution.

Analysis of single-molecule FRET results

FRET efficiency was approximated with $I_A/(I_A + I_D)$ (I_A: acceptor intensity and I_D: donor intensity) after each background was subtracted from donor and acceptor signals, and donor leakage was corrected. The background of each dye was acquired from the fluorescence intensity after both dyes were photobleached. The donor leakage was the ratio of acceptor intensity to donor intensity when only the acceptor dye was photobleached. The leakage was subtracted from the acceptor signal (29). Single-molecule FRET histograms were constructed by collecting FRET efficiencies of the first frame for ~4000 molecules. When we built up the histograms, outliers in total intensities ($I_A + I_D$) were excluded to guarantee the validity of FRET histograms. Then the peaks were fitted by multiple Gaussian functions by using commercial software (Origin 7.0, Origin Lab). The averaged background and donor leakage were used in this analysis, and therefore negative FRET efficiencies were seen. Using the first frame does not significantly mix different FRET states because all transition rates are less than $10\,s^{-1}$.

To analyze the dynamics of molecules, dwell-time and survival-time analyses were performed over 500 traces in one condition. For the dwell-time analysis, we collected the durations of staying in a FRET state and, for each state, constructed a duration histogram. When we built up the histograms, the bin size was set as a smaller value than the decay time. The histogram for each FRET state was fitted with an exponential decay function (Origin 7.0, Origin Lab.), and the corresponding decay time was treated as the dwell-time. The transition rate was obtained

by taking the inverse of the dwell-time. In the survival-time analysis, histograms were made for the lifetime of only single-FRET-state molecules before photo-bleaching. Each histogram was fitted with a single exponential function like the dwell-time analysis. The survival time indicates how long molecules can maintain one conformational state without a transition and does not provide the information on transition rates.

RESULTS

Ensemble measurements of single-base mutated human telomeric DNA motifs

To verify that our mutated HTDMs form G-quadruplex structures, ensemble CD and FRET measurements were done (Figure 1B and C). The CD spectra at 200 mM K^+ for the wild-type and mutated HTDMs are shown in Figure 1B. All spectra show a major peak at 295 nm, indicating that the mutated HTDMs fold into G-quadruplexes (30). For the CD measurements, only G-quadruplex motifs without fluorophores and a duplex stem were used as mentioned in 'Materials and Methods' section. In the single-molecule FRET experiments, it is possible that the dye modification and/or the duplex stem impede quadruplex formation. Ying *et al*. addressed this concern by conducting CD- and UV-melting experiments (27). In addition, we performed ensemble FRET measurements. The relative acceptor fluorescence of mutated HTDMs increased because of FRET as the K^+ concentration was elevated (Figure 1C and Supplementary Figure S1). This manifests that the distance between donor and acceptor dyes becomes shorter, and the mutated HTDMs fold into a more compact structure, G-quadruplex, by virtue of potassium ions (1–4). The CD and ensemble FRET results strongly support the idea that mutated HTDMs fold into G-quadruplexes.

Folded and unfolded states of the mutated human telomeric DNA motifs according to potassium concentrations

Single-molecule FRET histograms for the mutated HTDMs are shown as a function of K^+ concentrations at room temperature (Figure 2 and Supplementary Figure S2). These single-molecule FRET histograms of c-mut in Figure 2B were previously reported (22). The peak at zero is ignored because it results from donor-only labeled molecules due to faster photobleaching of acceptor (25). For all samples, at low K^+ concentrations, only a single peak with a low FRET efficiency (~0.25) was seen. As the K^+ concentration increases, higher FRET peaks become dominant, which is compatible with ensemble FRET results. In the absence of K^+, G-quadruplexes are barely formed and thus unfold. This unfolding increases the distance between donor and acceptor and, consequently, the FRET efficiency decreases. Therefore, the low FRET peak is assigned to the unfolded single-stranded overhang. Accordingly, the higher FRET peaks

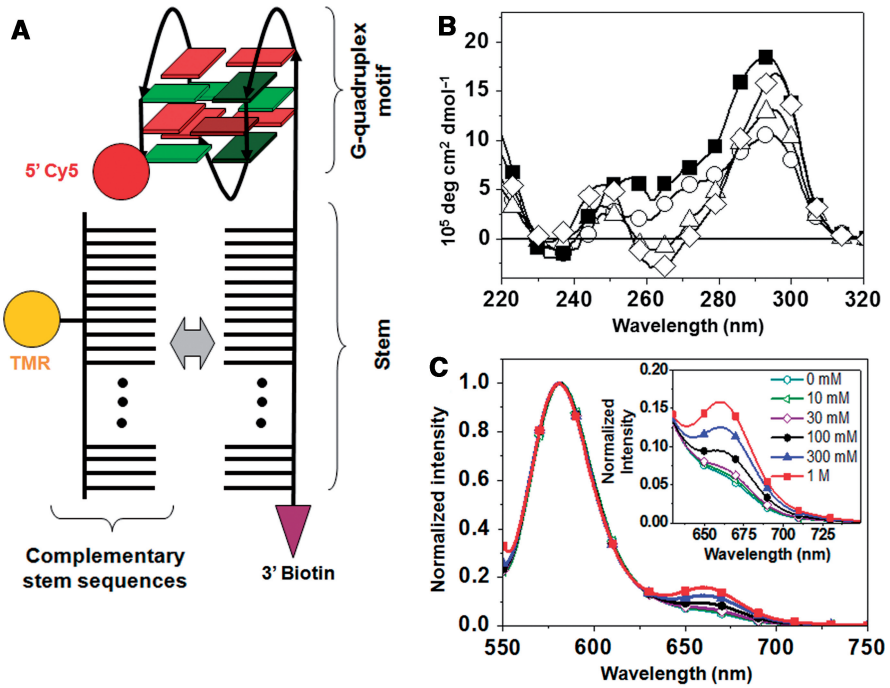

Figure 1. (**A**) A schematic diagram of sample which is composed of a single strand containing mutated human telomeric DNA motif (HTDM) and a double-stranded stem. Representatively, the quadruplex is depicted as the antiparallel conformation. The rectangles stand for guanines (green in syn and red in anti conformations). The mutated position is colored in dark green and dark red. Tetramethylrhodamine (TMR) for donor was internally labeled in stem strand, and Cy5 for acceptor was labeled at 5′- end of the HTDM. Biotin was modified at 3′-end of the HTDM for the surface immobilization. (**B**) Ensemble CD spectra in the presence of 200 mM K^+ at room temperature: (filled square) wild-type, (open circle) c-mut, (open diamond) s-mut1 and (open triangle) s-mut2. (**C**) Ensemble fluorescence spectroscopy at room temperature for c-mut at various K^+ concentrations. The spectra were normalized with TMR emission peak (580 nm). Inset: the zoom-in view of Cy5 emission spectra.

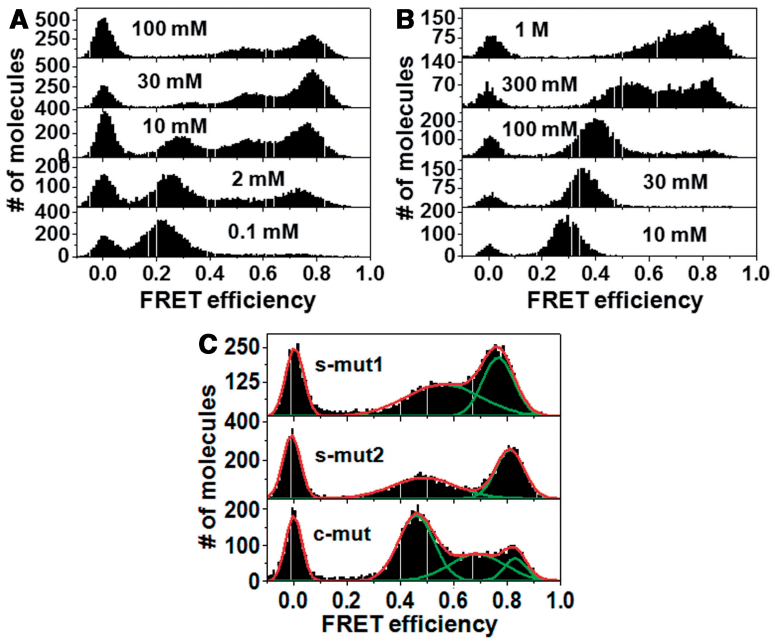

Figure 2. Single-molecule FRET histograms as a function of K^+ concentrations for the mutated HTDMs; (**A**) side-guanine (s-mut1) and (**B**) central-guanine (c-mut). The single-molecule FRET histograms of c-mut were previously reported (22). The peaks at zero result from donor-only molecules and hence are ignored. (**C**) Comparison of folded FRET peaks at 200 mM K^+ for each mutated HTDM (top: s-mut1, middle: s-mut2 and bottom: c-mut). All the peaks were fitted by multiple Gaussian functions. Two peaks in s-muts correspond to folded states. In c-mut, the low FRET peak (~0.45) represents an unfolded single-stranded overhang, and two other peaks correspond to folded states.

with FRET efficiencies invariant to K^+ concentrations, represent folded G-quadruplex structures. If we assume that the acceptor is located around the end of the duplex stem when the motif folds into the compact quadruplex, the distance between the donor and the acceptor is roughly estimated as 2.7–3.4 nm based on the double helix of DNA. This distance becomes shorter than the TMR-Cy5 Förster distance (~5.3 nm) (31) and thus the folded peaks could have FRET efficiency higher than 0.5. This is exactly consistent with the assignment of the wild type (22).

The unfolded peak of s-muts responds to the addition of K^+ differently from that of c-mut, as shown in Figure 2 and Supplementary Figure S2. The low FRET peak of the s-muts was significantly reduced at more than 30 mM K^+, where the folded peaks prevailed. In contrast, the low FRET peak of c-mut survived at 300 mM K^+ with a gradual movement toward higher FRET efficiency. This shift results from the increased flexibility of a single strand due to cation binding and/or screening to the negative charge of the DNA backbone (32). This behavior of the single strand was confirmed by Li^+ titration because Li^+ poorly stabilizes G-quadruplex (3,4). As Li^+ concentration increased, the unfolded peak also moved to a higher FRET efficiency gradually and was positioned at the same FRET efficiency as the low FRET peak at the same K^+ concentration (Supplementary Figure S7).

The population of unfolded peak is closely related to the instability of folded states. The unfolded peak of the wild type is almost suppressed at 10 mM K^+ (22). This result demonstrates that the G-quadruplexes of mutated HTDMs are less stable than those of the wild type. Moreover, the survival of the unfolded peak in c-mut at high K^+ concentrations indicates that the folded states of c-mut are less stable than those of s-muts.

On the other hand, two distinct folded peaks in each mutated HTDM were apparent at 200 mM K^+ (Figure 2C). In c-mut, the two folded peaks appeared around 0.7 (0.68 ± 0.09) and 0.8 (0.83 ± 0.04), besides the peak at 0.45 that corresponds to the unfolded states based on Li^+ titration (Supplementary Figure S7). In s-mut1, two folded peaks appeared around 0.6 (0.58 ± 0.11) and 0.8 (0.80 ± 0.05). In s-mut2, two folded peaks were shown around 0.5 (0.49 ± 0.11) and 0.8 (0.81 ± 0.05). This two-peak configuration and the peak positions do not change beyond 100 mM K^+, which supports our assignment that the higher peaks correspond to the folded states. Our mutated HTDMs exhibit one common conformation (FRET efficiency: 0.8) and three different conformations (FRET efficiencies: 0.5, 0.6 and 0.7) depending on the mutation position. It is important to note that there is a common peak regardless of the mutation position. Its FRET efficiency is about 0.8, which is the same as the efficiency of the folded peak in the wild-type at high K^+ concentration (22). This feature implies that the mutated HTDMs in which thymine is exchanged for guanine commonly have the potassium formation of the wild type. The folded peaks with FRET efficiencies lower than 0.8 probably represent conformations other than the potassium formation. To date, several conformations for HTDMs have been proposed, such as propeller-like all-parallel, anti-parallel fold-back and anti-parallel chair (33–35). Most recent studies reported that the potassium formation of the wild-type HTDMs is a

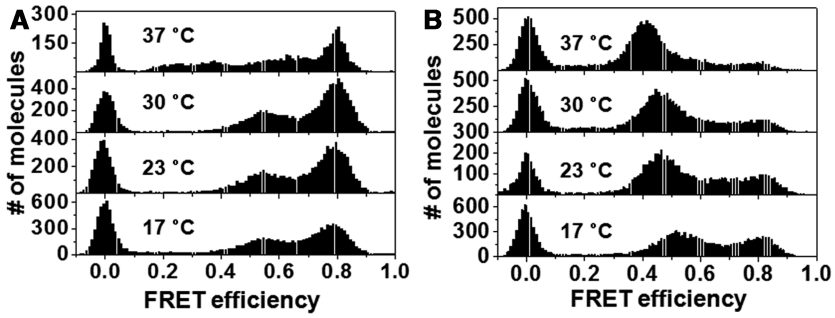

Figure 3. Temperature-dependent FRET histograms for (**A**) s-mut1 and (**B**) c-mut at 200 mM K^+. In s-mut1, the unfolded peak occurs at 37°C. Meanwhile, the unfolded peak of c-mut becomes dominant and moves to low FRET efficiency as temperature increases.

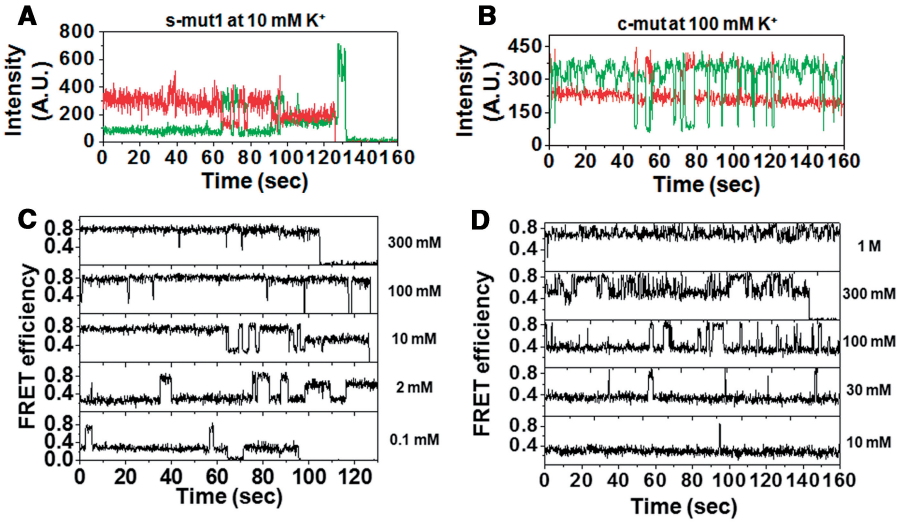

Figure 4. Single-molecule FRET time traces at room temperature (0.1 s integration time). Donor (green) and acceptor (red) intensities as a function of time for (**A**) s-mut1 at 10 mM K^+ and (**B**) c-mut at 100 mM K^+. FRET time traces of (**C**) s-mut1 and (**D**) c-mut according to K^+ concentrations. The time trace of c-mut at 300 mM K^+ was already reported in our earlier study (22). In the time traces of s-mut1 (0.1 mM K^+ and 100 mM K^+), transient zero FRET states, called blinking, were observed.

hybrid-type in which parallel and anti-parallel conformations are mixed (36,37). Even though we could not definitely resolve the conformations with our results, it is probable that the lower folded peaks arise from the proposed structures. Also, we cannot exclude the possibility that the mutated HTDMs fold into any peculiar structures.

Thermal effect on the equilibrium states

Thermal energy is one of factors that destabilize G-quadruplexes. We examined the thermal effect on the equilibrium states of the mutated HTDMs at physiological potassium concentration (200 mM). Temperature-dependent FRET histograms are shown for the mutated HTDMs in Figure 3 and Supplementary Figure S2. In c-mut, a rise in temperature depleted the folded states, and populated more unfolded states. The unfolded peak moved to a lower FRET with an increase in temperature because the thermal activation caused the end of the single strand with the acceptor to be farther away from the donor. For s-muts, folded peaks were prevalent regardless of temperature. The unfolded peak emerged at 37°C, whereas the unfolded peak of the wild-type does not appear even at 45°C (22). At the physiological salt concentration, the mutated HTDMs are more fragile to thermal agitation than the wild-type, and the central-G mutated HTDMs are more sensitive to temperature than the side-G mutated HTDMs.

Conformational dynamics of the single-base mutated G-quadruplexes

The conformational dynamics of the mutated HTDMs was directly observed at various K^+ concentrations from single-molecule time traces. These traces revealed the details of destabilization induced by the mutation (Figure 4 and Supplementary Figure S3). Figure 4A and B shows the time traces of fluorescence intensities for s-mut1 at 10 mM K^+ and c-mut at 100 mM K^+, respectively. In both traces, the anti-correlation between two fluorophores is apparent. In Figure 4A, acceptor and

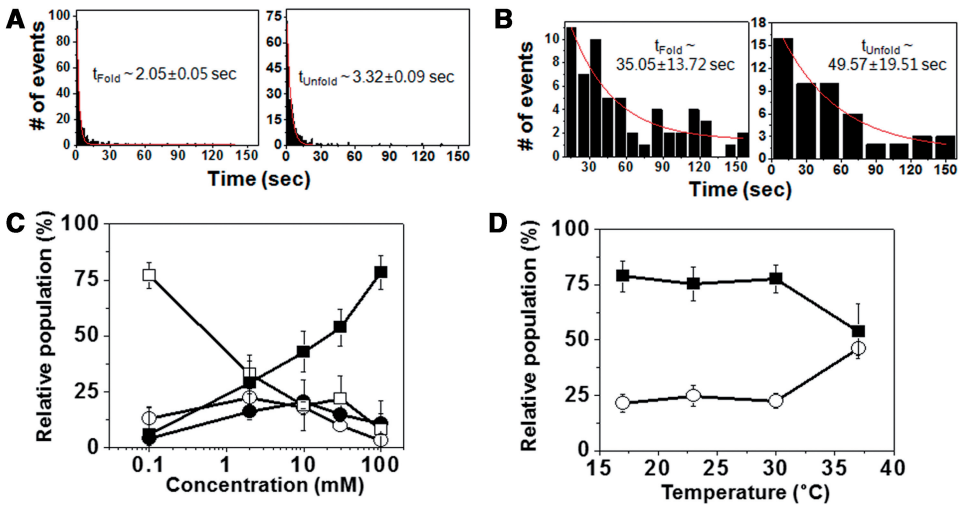

Figure 5. Heterogeneous dynamics in side-G mutated HTDMs (s-mut1). (**A**) The lifetimes of folded and unfolded states were obtained by the dwell-time analysis at 10 mM K^+. (**B**) The survival times of folded and unfolded states were derived from the survival-time analysis at 10 mM K^+. (**C**) Relative populations for four different dynamic species at room temperature according to K^+ concentration: (filled square) long-lived folded species, (open square) long-lived unfolded species, (filled circle) short-lived folded species and (open circle) short-lived unfolded species. (**D**) Temperature-dependent relative populations of (filled square) long-lived and (open circle) short-lived species at 200 mM K^+. The error bars in the relative populations were obtained from the confidence interval with 95% confidence level.

donor display single-step photobleaching sequentially, which is evidence that our experiments were performed at single-molecule level. In Figure 4C and D, FRET time traces are exhibited as a function of K^+ concentrations. Transient zero FRET states were observed in some time traces in Figure 4C (at ~63 s at 0.1 mM K^+ and at ~115 s at 100 mM K^+). This phenomenon, known as blinking, is random and reversible quenching of the donor or acceptor dye mainly due to the triplet states of fluorophores (38). This blinking also confirms that our experiments were done at single-molecule level. In the time traces, the molecules must pass through the low FRET state to transit into higher FRET states. This confirms our assignment of the low FRET to an unfolded single-stranded overhang. At low K^+ concentrations, the mutated HTDMs resided in the unfolded state and rarely folded. The addition of K^+ gradually curtailed the duration of unfolded state and facilitated the folding of the mutated molecules. At high K^+ concentrations, the dynamics of s-muts were dramatically different from that of c-mut. As reported in our previous work (22), c-mut fluctuated between folded and unfolded states rapidly and never held a folded state for a long time (Figure 4D). The appearance of the folded peaks in Figure 2B results from frequent foldings, or the reduced duration of unfolded states because a high K^+ concentration raises the probability that molecules take up the cations. In contrast, the folded states of s-muts were prolonged and occasionally unfolded for a short-time. It is noteworthy that the short unfoldings still exist at high K^+ concentrations, although they were not vivid in the FRET histograms. This result means that s-muts are not stabilized as robustly as the wild type, even when potassium ions are sufficient. Consequently, the conformational dynamics reveal that the replacement of single guanine by thymine never stabilizes the folded structures at the physiological K^+ concentration, even though only folded states were exhibited in the FRET histograms and bulk assays. In addition, the conformational dynamics are dramatically affected by the mutated position.

Heterogeneous dynamics of the side-G mutated human telomeric DNA motifs

In the side-G mutated HTDMs, two distinct dynamic behaviors were observed at an intermediate K^+ concentration (10 mM) (Figure 4C and Supplementary Figure S3). These behaviors were reported in our previous study about the wild-type HTDMs (22). Like the wild-type, some molecules occasionally stay in a folded (or unfolded) state for a long time. These molecules are termed long-lived species. Other molecules sometimes fluctuate quickly between folded and unfolded states and are termed short-lived species. In order to confirm this heterogeneous dynamics, dwell-time and survival-time analyses were performed for s-muts at 10 mM K^+ (see 'Materials and Methods' section for details). The survival time was obtained by collecting the lifetimes of molecules in a single state before fluorophores were photobleached. Thus, the survival time represents how long a molecule maintains a conformational state, without any transitions until dyes are photobleached. From the dwell-time analysis, the lifetimes of folded and unfolded states for s-mut1 were estimated as 2.05 s and 3.32 s, respectively (Figure 5A). The survival times of folded and unfolded states were 35.05 s and 49.57 s, respectively, which are ~15 times larger than the dwell times (Figure 5B). Similarly, the survival times of s-mut2 (folded: 30.21 s and unfolded: 41.17 s) are at least seven times larger than the dwell times (folded: 2.27 s and unfolded: 5.97 s) (Supplementary Figure S4). This significant

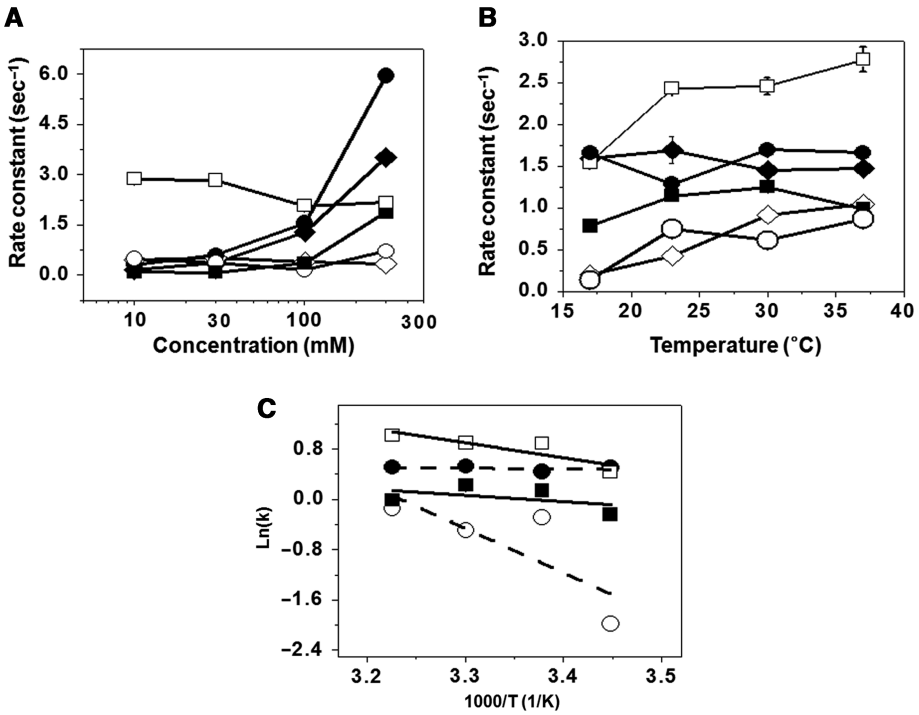

Figure 6. Transition rates between short-lived folded and unfolded states for s-mut1 and c-mut depending on (**A**) K^+ concentrations at room temperature and (**B**) temperature at 200 mM K^+. (Filled square) folding rate of c-mut, (open square) unfolding rate of c-mut, (filled circle) folding rate of s-mut1, (open circle) unfolding rate of s-mut1, (filled diamond) folding rate of s-mut2 and (open diamond) unfolding rate of s-mut2. The error bars were obtained from the fitting errors in the dwell-time analysis. (**C**) Arrhenius plots of the short-lived species of c-mut and s-mut1. (Filled square) folding of c-mut, (open square) unfolding c-mut, (filled circle) folding of s-mut1 and (open circle) unfolding of s-mut1. The activation energies (E_a) were obtained by a linear fitting; folding E_a of c-mut: 2.02 ± 2.60 kcal mol^{-1}, folding E_a of s-mut1: 0.28 ± 0.57 kcal mol^{-1}, unfolding E_a of c-mut: 4.69 ± 1.82 kcal mol^{-1}, and unfolding E_a of s-mut1: 13.52 ± 7.50 kcal mol^{-1}.

difference manifests the heterogeneity in the dynamics. With a criterion of ~30 s based on the survival times, we classified the dynamic states of the side-G mutated HTDMs into four species: long-lived folded, long-lived unfolded, short-lived folded and short-lived unfolded. We also tried to perform the survival-time analysis for c-mut, but we could not obtain statistically meaningful data because c-mut molecules showing only one folded state before photobleaching were very rare.

In Figure 5C and Supplementary Figure S5A, the relative population of each species of s-muts is shown as a function of K^+ concentration. The trend of conformational dynamics in time traces (Figure 4C and Supplementary Figure S3) is well reflected in these results. Long-lived folded and long-lived unfolded species were dominant at high and low K^+ concentrations, respectively. The short-lived species were maximally populated at intermediate concentrations. This change of relative populations, which were obtained from relative durations in each state, is also consistent with the single-molecule histograms constructed from many different molecules at one time. This manifests that our molecular system is ergodic. Moreover, no direct transitions between long-lived folded and long-lived unfolded species were witnessed. This result implies that the short-lived species act as a mediator bridging the two long-lived species. Figure 5D and Supplementary Figure S5B show temperature dependence of the relative population for long-lived species and short-lived species of s-muts at 200 mM K^+. At 37°C, the population of short-lived species abruptly increases (~40%), and the long-lived species are depopulated. The increase of short-lived species indicates that the G-quadruplexes of s-muts become more unstable at 37°C. This increased instability may account for the appearance of unfolded peak at 37°C in the single-molecule FRET histograms (Figure 3A and Supplementary Figure S2).

Kinetics of short-lived species of the mutated human telomeric DNA motifs

We investigated the kinetics of short-lived species in the mutated HTDMs because the short-lived species play a key role in the overall kinetics; they serve as a mediator in s-muts and are the majority in c-mut. Figure 6A presents the transition rates of short-lived species according to K^+ concentration. The unfolding rates are invariant with respect to K^+ concentrations, meaning that the folded states of short-lived species are energetically unaffected by the addition of K^+ and, furthermore, implying that the number of potassium ions associated with short-lived folded states are limited. The unfolding rate of c-mut is about four times larger than that of s-muts, which indicates that the stability of short-lived folded species is greater than in s-muts than in c-mut. On the other hand, folding rates increase with the addition of K^+, because the binding of cations is more feasible at

high concentration. Notably, the folding rates of s-muts increase more rapidly and are larger than those of c-mut. This feature demonstrates that the potassium ions are more favorably coordinated in s-muts than in c-mut. For a more quantitative understanding of the energy barriers, the temperature dependence of rate constants was examined at the physiological potassium concentration (200 mM) (Figure 6B). Overall, the transition rates are insensitive to temperature compared with K^+ titration. The activation energies of short-lived species of the mutated HTDMs were obtained from Arrhenius plot (Figure 6C and Supplementary Figure S6). The folding activation energies of short-lived species are 2.02 ± 2.60 kcal mol^{-1}, 0.28 ± 0.57 kcal mol^{-1} and 0.12 ± 0.42 kcal mol^{-1} for c-mut, s-mut1 and s-mut2, respectively. The folding energy barriers of c-mut and s-muts are not significantly different and are small. Such small energy barrier means that the folding energy barrier of the mutated HTDMs is entropic rather than enthalpic. On the contrary, the unfolding activation energies of c-mut, s-mut1 and s-mut2 are 4.69 ± 1.82 kcal mol^{-1}, 13.52 ± 7.50 kcal mol^{-1} and 15.13 ± 2.94 kcal mol^{-1}, respectively. The unfolding barriers of s-mut1 and s-mut2 are similar to each other and are about three-fold higher than that of c-mut. In other words, 3-fold higher energy is required for the short-lived folded states of s-muts to unfold than for those of c-mut. This shows, quantitatively, that the short-lived folded states of s-muts are more stable than those of c-mut energetically.

DISCUSSION

We observed that the replacement of guanine by thymine in a G-tetrad destabilizes the stable G-quadruplex structure and that the conformational dynamics of the mutated HTDMs depends on the mutation position. The central-G mutated HTDM is severely destabilized even at high K^+ concentrations. On the other hand, the side-G mutated HDTMs are less stable than the wild type and more stable than c-mut. They also show heterogeneous dynamics like the wild type. This destabilization arises because the substitution of thymine disturbs the various molecular interactions to stabilize G-quadruplexes, such as Hoogsteen hydrogen bonding, base-stacking interaction, and K^+ coordination between G-tetrads (39,40). We speculate on the mechanisms by which the substituted thymine destabilizes G-quadruplexes. First, thymine cannot form the cyclic Hoogsteen bonding with its neighboring guanines. Thus, the disruption of hydrogen bonds due to the thymine weakens the stability of G-quadruplexes. Both c-mut and s-muts have breakage of hydrogen bonds in each G-tetrad. But s-muts are not destabilized as severely as c-mut at high K^+ concentrations. This indicates that the breakage of hydrogen bonds is not a critical factor in causing the different dynamics between c-mut and s-muts. Moreover, the disruption of hydrogen bonding due to the substituted thymine can break the symmetry of a G-tetrad, and the well-organized guanine stacks will be disturbed. The base-stacking interaction is one of the crucial factors to stabilize G-quadruplexes like single- or double-stranded DNA (39,40). The base-stacking interaction is sensitive to the geometry and alignment between bases because the interaction is made of the London dispersion force and hydrophobic interaction (41). The disruption of guanine stacks due to the thymine weakens the stacking interaction and destabilizes the G-quadruplexes. Moreover, the base-stacking interaction will be changed depending on the thymine position in a G-track. The thymine in c-mut, which is in the middle quartet, has base-base interactions with two guanines in the upper and lower quartets, whereas the thymine in s-muts is placed in the outer quartet and interacts with only one guanine. Consequently, the thymine position in a G-track will give rise to the different degree of stability between c-mut and s-muts. Finally, the potassium coordination can affect the destabilization of mutated HTDMs. The stability of G-quadruplexes is closely related to monovalent cations that are coordinated between quartets. The cations that are coordinated precisely in the cavities of G-quadruplexes have the cation-dipole interaction with eight carbonyl oxygen-6 atoms in guanines (1–4). Among monovalent cations, potassium ion is known to stabilize the wild-type G-quadruplexes most strongly (3,4). The wild-type G-quadruplexes are destabilized when cations cannot be properly coordinated. When potassium ions are insufficient, or only weakly coordinated cations such as Li^+ are present, the G-quadruplexes are unstable. Likewise, potassium ions cannot be precisely coordinated because the substituted thymine in the mutated HTDMs changes the configuration of the cation-dipole interaction. Consequently, this imperfect potassium coordination destabilizes the mutated G-quadruplexes. Furthermore, the imperfect coordination can explain the dependence of dynamics on the mutation position like the base-stacking interaction. It is known that the wild-type human telomeric G-quadruplex contains two coordinated potassium ions in its cavities (2,36). If this is true for the mutated HTDMs, the mutation at the middle quartet in c-mut influences the two potassium ions in both upper and lower cavities simultaneously. Hence, neither of them can be precisely coordinated to the cavities. Meanwhile, when the side-G mutated HTDMs form the G-quadruplexes, the thymine would belong to either the top or bottom quartet and thus affect the coordination of only one cation. The one perfect coordination definitely increases stability relative to c-mut.

Even though base-stacking and potassium coordination affect the stability of G-quadruplexes dominantly, we cannot exclude factors associated with uncoordinated K^+ for the higher stability of s-muts. The monovalent cations reduce the electrostatic repulsion for the compact structure. Moreover, the extra potassium ions can interact with loops. In *Oxytricha nova* telomeric G-quadruplex, the cations are coordinated between thymines in a loop and an outer quartet (42,43). For the human telomeric G-quadruplexes, it was proposed that potassium ions can be coordinated with edge-wise loops (44). Such interactions may compensate for the disorder of base-stack and imprecise coordination in an outer G-tetrad and induce a transition from the short-lived to the long-lived species

in s-muts. But they appear to be insufficient to stabilize the central-G mutated G-quadruplex.

CONCLUSIONS

We observed that the degree of destabilization depends on the mutation position in a G-track as reported previously (21). By using single-molecule FRET spectroscopy, we also found that the mutated HTDMs, in which thymine is exchanged for guanine, have structural polymorphism and are destabilized to encourage short-lived species at the physiological K^+ concentration. Furthermore, we uncovered many of details in conformational dynamics of the mutated HTDMs. In the central-G mutated HTDM, the short-lived species were predominantly populated, whereas the side-G mutated HTDMs displayed heterogeneous dynamics with both long- and short-lived species. We speculate that this is because a guanine in a middle quartet interacts with both upper and lower G-tetrads via base-stacking interaction and is involved in the coordination of two potassium ions.

The stability of quadruplex structures may be crucial for maintaining normal biological processes or genomic integrity inside a cell. Our results demonstrate that the replacement of only single guanine in a G-track dramatically disrupts the stability of human telomeric G-quadruplexes. This demonstration can offer an insight on biological phenomena and abnormalities associated with G-quadruplexes, in several genomic regions as well as telomeres. Moreover, the details about the kinetics and structural polymorphism of the mutated HTDMs will provide information that is beneficial for the design of ligands that stabilize the mutated G-quadruplex as well as the wild-type.

SUPPLEMENTARY DATA

Supplementary Data are available at NAR Online.

ACKNOWLEDGEMENTS

We thank Professor T. Ha of Howard Hughes Medical Institute and Department of Physics, University Illinois for helpful discussion and support. We also thank Professor S. Hohng of Department of Physics and Astronomy, Seoul National University for thoughtful discussion and supports and also for the generous provision of utilities.

FUNDING

Korean government [Korea Science and Engineering Foundation (KOSEF)]; Ministry of Education, Science and Technology (MEST, R11-2008-095-01000-0); Seoul R&BD and KRF (Grant Nos. C00012 and C00032); Ministry of Knowledge Economy (MKE).

Conflict of interest statement. None declared.

REFERENCES

1. Keniry,M.A. (2001) Quadruplex structures in nucleic acids. *Biopolymers*, **56**, 123–146.
2. Burge,S., Parkinson,G.N., Hazel,P., Todd,A.K. and Neidle,S. (2006) Quadruplex DNA: sequence, topology, and structure. *Nucleic Acid Res.*, **34**, 5402–5415.
3. Simonsson,T. (2001) G-quadruplex DNA structures-variation on a theme. *Biol. Chem.*, **382**, 621–628.
4. Davis,J.F. (2004) G-quartets 40 years later: from 5'GMP to molecular biology and supramolecular chemistry. *Angew. Chem. In. Ed.*, **43**, 668–698.
5. Neidle,S. and Read,M.A. (2001) G-quadruplexes as therapeutic targets. *Biopolymers*, **56**, 195–208.
6. Schaffitzel,C., Berger,I., Postberg,J., Hanes,J., Lipps,H.J. and Pluckthun,A. (2001) In vitro generated antibodies specific for telomeric guanine-quadruplex DNA react with Stylonychia lemnae macronuclei. *Proc. Natl Acad. Sci. USA*, **98**, 8572–8577.
7. Paeschke,K., Simonsson,T., Vincent,J.A., Taylor,A.F. and Maizels,N. (2004) Intracellular transcription of G-rich DNAs induces formation of G-loops, novel structures containing G4 DNA. *Genes Dev.*, **18**, 1618–1629.
8. Siddiqui-Jain,A., Grand,C.L., Bearss,D.J. and Hurley,L.H. (2002) Direct evidence for a G-quadruplex in a promoter region and its targeting with a small molecule to repress c-MYC transcription. *Proc. Natl Acad. Sci. USA*, **99**, 11593–11598.
9. Neidle,S. and Parkinson,G.N. (2003) The structure of telomeric DNA. *Curr. Opin. Struc. Biol.*, **13**, 275–283.
10. Tang,J., Kan,Z., Yao,Y., Wang,Q., Hao,Y. and Tan,Z. (2008) G-quadruplex preferentially forms at the very 3′ end of vertebrate telomeric DNA. *Nucleic Acid Res.*, **36**, 1200–1208.
11. Zakian,V.A. (1995) Telomeres: Beginning to understand the end. *Science*, **270**, 1601–1607.
12. Neidle,S. and Parkinson,G.N. (2002) Telomere maintenance as a target for anticancer drug discovery. *Nat. Rev. Drug Discovery*, **1**, 383–393.
13. Cian,A.D., Lacroix,L., Douarre,C., Smaali,N.T-., Trentesaux,C., Riou,J-.F and Mergny,J-.L. (2008) Targeting telomeres and telomerase. *Biochimie*, **90**, 131–155.
14. Zahler,A., Williamson,J.R., Cech,T.R. and Prescott,D.M. (1991) Inhibition of telomerase by G-quartet DNA structures. *Nature*, **350**, 718–720.
15. Rezler,E.M., Bearss,D.J. and Hurley,L.H. (2002) Telomeres and telomerases as drug targets. *Curr. Opin. Pharmacol.*, **2**, 415–423.
16. Simonsson,T., Pecinka,P. and Kubista,M. (1998) DNA tetraplex formation in the control region of c-myc. *Nucleic Acid Res.*, **26**, 1167–1172.
17. Rankin,S., Reszka,A.P., Huppert,J., Zloh,M., Parkinson,G.N., Todd,A.K., Ladame,S., Balasubramanian,S. and Neidle,S. (2005) Putative DNA quadruplex formation within human c-kit oncogene. *J. Am. Chem. Soc.*, **127**, 10584–10589.
18. Sen,D. and Gilbert,W. (1988) Formation of parallel four-stranded complexes by guanine-rich motifs in DNA and its implications for meiosis. *Nature*, **334**, 364–366.
19. Catasti,P., Chen,X., Moyzis,R.K., Bradbury,E.M. and Gupta,G. (1996) Structure-function correlations of the insulin-linked polymorphic region. *J. Mol. Biol.*, **264**, 534–545.
20. Grand,C.L., Powell,T.J., Nagle,R.B., Bearss,D.J., Tye,D., Guzman,M.G. and Hurley,L.H. (2004) Mutations in the G-quadruplex silencer element and their relationship to c-MYC overexpression, NM23 repression and therapeutic rescue. *Proc. Natl Acad. Sci. USA*, **101**, 6140–6144.
21. Mekmaysy,C.S., Petraccone,L., Garbett,N.C., Ragazzon,P.A., Gray,R., Trent,J.O. and Chaires,J.B. (2008) Effect of O^6-methylguanine on the stability of G-quadruplex DNA. *J. Am. Chem. Soc.*, **130**, 6710–6711.
22. Lee,J.Y., Okumus,B., Kim,D.S. and Ha,T. (2005) Extreme conformational diversity in human telomeric DNA. *Proc. Natl Acad. Sci. USA*, **102**, 18938–18943.
23. Albert,B., Bray,D., Hopkin,K., Johnson,A., Lewis,J., Raff,M., Robert,K. and Walter,P. (2004) *Essential Cell Biology*, 2nd edn, p 390, Garland Science, NY.
24. Selvin,P.R. and Ha,T. (2007) *Single-Molecule Techniques – A Laboratory Manual*. Cold Spring Harbor Laboratory Press, NY.

25. Weiss,S. (1999) Fluorescence spectroscopy of single biomolecules. *Science*, **283**, 1676–1683.
26. Cornish,P.V. and Ha,T. (2007) A survey of single-molecule techniques in chemical biology. *ACS Chem. Biol.*, **2**, 53–61.
27. Ying,L., Green,J.J., Li,H., Klenerman,D. and Balasubramanian,S. (2003) Studies on the structure and dynamics of the human telomeric G-quadruplex by single-molecule fluorescence resonance energy transfer. *Proc. Natl Acad. Sci. USA*, **100**, 14629–14634.
28. Benesch,R.E. and Benesch,R. (1953) Enzymatic removal of oxygen for polarography and related methods. *Science*, **118**, 447–448.
29. Sabanayagam,C.R., Eid,J.S. and Meller,A. (2005) Using fluorescence resonance energy transfer to measure distances along individual DNA molecules: Corrections due to nonideal transfer. *J. Chem. Phys.*, **122**, 061103.
30. Qi,J. and Shafer,R.H. (2005) Covalent ligation studies on the human telomere quadruplex. *Nucleic Acid Res.*, **33**, 3185–3192.
31. Deniz,A.A., Dahan,M., Grunwell,J.R., Ha,T., Faulhaber,A.E., Chemla,D.S., Weiss,S. and Schultz,P.G. (1999) Single-pair fluorescence resonance energy transfer on freely diffusing molecules: Observation of Förster distance dependence and subpopulations. *Proc. Natl Acad. Sci. USA*, **96**, 3680–3675.
32. Murphy,M.C., Rasnik,I., Cheng,W., Lohman,T.M. and Ha,T. (2004) Probing single-stranded DNA conformational flexibility using fluorescence spectroscopy. *Biophysical J.*, **86**, 2530–2537.
33. Wang,Y. and Patel,D.J. (1993) Solution structure of the human telomeric repeat d[AG3(T2AG3)3] G-tetraplex. *Structure*, **1**, 263–282.
34. Parkinson,G.N., Lee,M.P.H. and Neidle,S. (2002) Crystal structure of parallel quadruplexes from human Telomeric DNA. *Nature*, **417**, 876–880.
35. He,Y., Neumann,R.D. and Panyutin,I.G. (2004) Intramolecular quardruplex conformation of human telomeric DNA assessed with ^{125}I-radioprobing. *Nucleic Acid Res.*, **31**, 5359–5367.
36. Ambrus,A., Chen,D., Dai,J., Bialis,T., Jones,R.A. and Yang,D. (2006) Human telomeric sequence forms a hybrid-type intramolecular G-quadurplex structure with mixed parallel/antiparallel strands in potassium solution. *Nucleic Acid Res.*, **34**, 2723–2735.
37. Dai,J., Carver,M., Puchihewa,C., Jones,R.A. and Yang,D. (2007) Structure of the hybrid-2 type intramolecular human telomeric G-quadruplex in K^+ solution: insights into structure polymorphism of the human telomeric sequence. *Nucleic Acid Res.*, **35**, 4927–4940.
38. Sabanayagam,C.R., Eid,J.S. and Meller,A. (2005) Long time scale blinking kinetics of cyanine fluorophores conjugated to DNA and its effect on Förster resonance energy transfer. *J. Chem. Phys.*, **123**, 224708.
39. Olsen,C.M., Gmeiner,W.H. and Marky,L.A. (2006) Unfolding of G-quadruplexes: energetic, and ion and water contributions of G-quartet stacking. *J. Phys. Chem. B.*, **110**, 6962–6969.
40. Olsen,C.H., Gmeiner,W.H. and Marky,L.A. (2008) Unfolding thermodynamics of interamolecular G-quadruplexes: base sequence contributions of the loops. *J. Phys. Chem. B.*, **113**, 2587–2595.
41. Müller-Dethlefs,K. and Hobza,P. (2000) Noncovalent interactions: a challenge for experiment and theory. *Chem. Rev.*, **100**, 143–167.
42. Haider,S., Parkinson,G.N. and Neidle,S. (2002) Crystal structure of the potassium form of an *Oxytricha nova* G-quadruplex. *J. Mol. Biol.*, **320**, 189–200.
43. Cevec,M. and Plavec,J. (2005) Role of loop residues and cations on the formation and stability of dimeric DNA G-quadruplexes. *Biochemistry*, **44**, 15238–15246.
44. Phan,A.T, Kuryavyi,V., Luu,K.N. and Patel,D.J. (2007) Structure of two intramolecular G-quadruplexes formed by natural human telomere sequences in K^+ solution. *Nucleic Acid Res.*, **35**, 6517–6525.